Marine Geology 410 (2019) 22–31

Contents lists available at ScienceDirect

Marine Geology

journal homepage: www.elsevier.com/locate/margo

The hiding-exposure effect revisited: A method to calculate the mobility of bimodal sediment mixtures

Connor J. McCarron[a,*], Katrien J.J. Van Landeghem[a], Jaco H. Baas[a], Laurent O. Amoudry[b], Jonathan Malarkey[a,c]

[a] School of Ocean Sciences, Bangor University, Menai Bridge, Anglesey LL59 5AB, UK
[b] National Oceanography Centre, Joseph Proudman Building, Liverpool L3 5DA, UK
[c] Energy and Environment Institute, University of Hull, Hull HU 7RX, UK

Keywords:
Hiding-exposure effect
Selective entrainment
Mixed sand-gravel
Flume experiments
Threshold of motion
Bedload transport

ARTICLE INFO

Editor: G.J. de Lange

ABSTRACT

Predicting seabed mobility is hampered by the limited accuracy of sediment transport models when the bed is composed of mixed sediments. The hiding-exposure (HE) effect modifies the threshold of motion of individual grain classes in sediment mixtures and its strength is dependent on the grain size distribution. However, an appropriate method of predicting this effect for bimodal sediment mixtures remains to be developed. The prototypical example of a bimodal mixture is that consisting of a well-sorted sand and gravel for the fine and coarse fractions respectively. Through a comprehensive series of laboratory experiments, the HE effect has been quantified for a full range of sand-gravel mixtures from pure sand to pure gravel, the choice of which has been underpinned by an integrated study of offshore geophysical and sedimentological data found in coastal and shelf seas. In the sand–gravel mixtures used in the present study the critical shear stress needed to mobilise the sand and gravel fractions increased by up to 75% and decreased by up to 64%, respectively, compared to that needed to mobilise well-sorted sediment of similar size. The HE effect was found to be dependent on the percentage of gravel (coarse mode) present in the bimodal mixture, whereby the effect for the mixture is the weighted sum of the HE effect for the fine and coarse modes.

1. Introduction

Sediment composition and transport are amongst the main controlling factors on seabed functioning in coastal and shelf seas. Engineering activity is widespread in these environments with the development of energy infrastructure and the need to mitigate against coastal hazards. The presence of structures associated with, for example, renewable energy and hydrocarbon extraction, can cause disturbance to natural sediment transport dynamics. In turn, this may have undesirable consequences, including damage of pipelines or subsea cables and scouring of the bed around man-made structures (e.g. Sumer et al., 2001).

Predicting the spatial variability of mixed seabed composition aids resource management, conservation and spatial planning (e.g. Warner et al., 2008a; Stephens and Diesing, 2015; Ward et al., 2015). Seabed sediment also supports benthic marine communities, acts as a sink for bacteria, pathogens, heavy metals and microplastics (e.g. James, 2002; Malham et al., 2014; Diesing et al., 2017; Ling et al., 2017), and carbon cycling is controlled by the heterogeneity of seafloor biota (Snelgrove et al., 2018). The mobility of seafloor sediment and resulting bedforms may also obstruct navigation channels (e.g. Aliotta and Perillo, 1987; Redding, 2000; Knaapen and Hulscher, 2002; Wienberg and Hebbeln, 2005), may dictate the sustainability of aggregate extraction (e.g. Le Bot et al., 2010; Van Lancker et al., 2010), and influence the recovery rate of the bed after demersal fishing activities (e.g. Diesing et al., 2013; Hiddink et al., 2017). The ability to accurately predict sediment

* Corresponding author.
E-mail address: c.j.mccarron@bangor.ac.uk (C.J. McCarron).

https://doi.org/10.1016/j.margeo.2018.12.001
Received 28 June 2018; Received in revised form 16 November 2018; Accepted 4 December 2018
Available online 11 December 2018

transport rates and pathways allows for better determination of seabed recovery rates, the potential for coastal erosion and the reconstruction of paleo-environments.

Insight into the dynamic processes governing sediment transport and the resulting seafloor morphological features therefore has implications for a wide range coastal and shelf sea stakeholders, for example: (1) companies assessing the safety of offshore structures and the sustainability of aggregate extraction; (2) seabed modellers predicting habitat resilience, pollutant dispersal and carbon fluxes; (3) planning authorities, coastal engineers and environmental advisers/managers, responsible for coastal erosion measures; (4) geoscientists conducting paleo-environmental reconstruction; and (5) the wider public as consumers of shelf sea resources (i.e. food, aggregates, fossil fuels and renewable energy). Hence, increased importance has been placed on the ability to predict the mobility of seabed sediment. The level of uncertainty is highest when the seabed consists of mixed sediment (Wilson et al., 2018), introduced to shelf and coastal seas by glacial and fluvial processes (Holland and Elmore, 2008). With this in mind the present study seeks to investigate the hiding-exposure function of a bimodal sediment distribution through detailed laboratory experiments. Hiding-exposure functions modify the critical shear stress for sediment movement for each size class in mixtures of sizes.

1.1. Predicting bedload transport

Bedload transport is the dominant mechanism controlling seabed morphodynamics. It occurs through the movement of sediment by the frictional force exerted by a flow per unit area on the seabed, referred to as the bed shear stress, τ:

$$\tau = \rho u_*^2, \tag{1}$$

where ρ is the density of water and u_* is the friction velocity. Once τ exceeds the critical shear stress, τ_{cr}, grains begin to move. Often, τ and τ_{cr} are expressed in dimensionless form as the Shields (1936) parameter, θ, and critical Shields parameter, θ_{cr}, respectively:

$$\theta = \frac{\tau}{\rho g(s-1)d_n}, \qquad \theta_{cr} = \frac{\tau_{cr}}{\rho g(s-1)d_n}, \tag{2a,b}$$

where g is the acceleration due to gravity, $s = \rho_s / \rho$ is the specific density of the sediment, ρ_s is the sediment density, and d_n is a representative grain size (i.e. the median grain size, d_{50}, or mean grain size, d_m). A wide range of formulae have been developed theoretically and empirically to predict bedload transport rates (e.g. Meyer-Peter and Müller, 1948; Einstein, 1950; Bagnold, 1956, 1966; Yalin, 1963; Engelund and Hansen, 1967; Ashida and Michiue, 1971; Engelund and Fredsøe, 1976; van Rijn, 1984; Nielsen, 1992). These equations relate the dimensionless bedload transport rate, $q_b{}^*$, to some function of the excess Shields parameter ($\theta - \theta_{cr}$)

$$q_b{}^* \equiv \frac{q_b}{[g(s-1)d_n{}^3]^{1/2}} = f(\theta - \theta_{cr}), \tag{3}$$

where q_b is the dimensional volumetric transport rate ($m^2 s^{-1}$). Eq. (3) is routinely applied in coastal sediment transport models to predict bedload transport rates (e.g. Lesser et al., 2004; Warner et al., 2008b). Eqs. (2a,b) and (3) assume a homogeneous grain size distribution represented by a single grain size (i.e. d_{50} or d_m) and might not be reflective of environments where sediment mixtures are composed of two or more sediment size classes. Single-class bedload transport equations have been adapted to account for multiple classes by separating the mixture into different grain size classes and calculating $q_{b,i}{}^*$, θ_i and $\theta_{cr,i}$ for each class (e.g. Meyer-Peter and Müller, 1948; van Rijn, 1984, 2007):

$$q_{b,i}{}^* = f(\theta_i - \theta_{cr,i}), \tag{4}$$

$$\theta_i = \frac{\tau_i}{\rho g(s-1)d_i}, \quad \theta_{cr,i} = \frac{\tau_{cr,i}}{\rho g(s-1)d_i}, \tag{5a,b}$$

where the subscript i refers to the i^{th} grain size class of the bed material.

1.2. The hiding-exposure effect

In equally sized sediment, transport is controlled by the absolute grain size of the bed material (e.g. Wilcock, 1993, 2001; Wilcock and Kenworthy, 2002). In mixed sediment, the differently sized grains interact uniquely with the flow leading to selective entrainment and this complicates the calculation of bedload transport rates. This selective entrainment is referred to as the hiding-exposure effect and describes the process in which small grains are hidden from a current by larger, more exposed grains. Hiding of grains in sediment mixtures results in an increase in the critical shear stress required to mobilise smaller grains. Exposure of grains leads to a decrease in the critical shear stress required to move large grains (Einstein, 1950). A correction factor, ξ_i, adjusts the critical Shields parameter, $\theta_{cr,i}$, of a particular grain size fraction as a function of its size relative to the median grain size of the mixture, d_i/d_{50} (Einstein, 1950; Wilcock, 1993):

$$\xi_i \equiv \frac{\theta_{cr,i}}{\theta_{cr,50}} = n\left(\frac{d_i}{d_{50}}\right)^{-\gamma}. \tag{6}$$

The exponent γ controls the strength of the hiding-exposure effect by modifying ξ_i for a given value of d_i/d_{50}, where γ ranges from 0 to 1.25 (Buffington and Montgomery, 1997, 1998) and $n = 1$ for sediment classes with the same density. Eq. (6) is used to adjust the critical Shields parameter for the initiation of motion in the dimensionless fractional bedload transport equation

$$q_{b,i}{}^* = f(\theta_i, \xi_i \theta_{cr,i}). \tag{7}$$

1.3. Predictive ability of currently used HE corrections

Several corrective equations use an approach similar to Eq. (6) (e.g. Egiazaroff, 1965; Ashida and Michiue, 1971; Hayashi et al., 1980; Parker et al., 1982; Wilcock and Crowe, 2003) (Table 1). Following Eq. (6), the degree of variation in γ is a function of the variation of $\tau_{cr,i}/\tau_{cr,50}$. Shvidchenko et al. (2001) demonstrated that, for unimodal and weakly bimodal sediments, γ is dependent on d_{50} and to a lesser extent on the geometric standard deviation, σ_g,

$$\gamma = 2\sigma_g{}^{-0.10}(0.049l^3 - 0.26l^2 + 0.33l + 1.20) - 1.4, \tag{8}$$

where $l = \log(d_{50})$ and d_{50} in is mm. In bimodal sediment, $\tau_{cr,i}/\tau_{cr,50}$ has been shown to be dependent on relative size effects with $0 < \gamma < 1$ (e.g. Wilcock, 1993; Kleinhans and van Rijn, 2002). Wilcock (1993) proposed a bimodality index, B, to quantify the degree of bimodality in sediment mixtures and Sambrook Smith et al. (1997) proposed a modified bimodality index B^* to account for the relative magnitude of different modes:

Table 1
Hiding exposure formulae.

Author	Formula
Egiazaroff (1965)	$\xi_i = \left[\frac{\log(19)}{\log(19 d_i / d_{50})}\right]^2$
Ashida and Michiue (1973)	$\xi_i = \begin{cases} 0.85(d_i/d_{50})^{-1} & \text{For } d_i/d_{50} < 0.40 \\ \left[\frac{\log(19)}{\log(19 d_i/d_{50})}\right]^2 & \text{For } d_i/d_{50} > 0.40 \end{cases}$
Hayashi et al. (1980)	$\xi_i = \begin{cases} (d_i/d_m)^{-1} & \text{For } d_i/d_{50} < 1.0 \\ \left[\frac{\log(8)}{\log(8 d_i/d_m)}\right]^2 & \text{For } d_i/d_{50} > 1.0 \end{cases}$
Parker et al. (1982)	$\xi_i = (d_i/d_{50})^{-0.982}$
Wilcock and Crowe (2003)	$\xi_i = (d_i/d_{50})^{-\gamma} \quad \gamma = 1 - \frac{0.67}{1+\exp(1.5 - d_i/d_{50})}$

Where $\xi_i = \theta_{cr,\,i}/\theta_{cr,\,50}$

$$B = (d_c/d_f)^{1/2}(f_c + f_f), \quad B^* = |\Phi_2 - \Phi_1|(f_2/f_1), \tag{9a,b}$$

where d_c and d_f, are the grain sizes of the coarse and fine modes respectively, and f_c and f_f, are the fractions of the coarse and fine modes respectively in Eq. (9a). In Eq. (9b), Sambrook Smith et al. (1997) define the grain size of the modes in Φ-units so that B^* approaches zero as the separation between the two modes vanishes, and define the two modes according to their amplitude rather than grain size where: Φ_1 and Φ_2 are the grain sizes, in phi units, of the primary and secondary modes respectively; and f_1 and f_2 are the fractions of the primary and secondary modes respectively. In both Eqs. (9a,b), a mode is defined as four continuous quarter-Φ grain classes containing the mode. In Eq. (9b), if both modes are of equal amplitude, the primary mode refers to the coarser mode.

Wilcock (1993) and Sambrook Smith et al. (1997) defined γ in Eq. (6) according to:

$$\gamma = (1 - 1.7/B), \quad \gamma = (1 - 1.5/B^*), \tag{10a,b}$$

where $B > 1.7$ and $B^* > 1.5$. The correlation between γ and B or B^* has not been found to be strong (e.g. Kuhnle, 1992, 1993a, 1993b; Wilcock, 1993). Patel et al. (2013) was critical of these expressions because they could only represent bimodal distributions and instead prescribed γ in terms of σ_g

$$\gamma = \begin{cases} 0.96, & \sigma_g < 2.85, \\ 2.67\exp(-0.37\sigma_g), & \sigma_g \geq 2.85, \end{cases} \tag{11}$$

such that when $\sigma_g < 2.85$, the distribution is unimodal. However, there is still no generally accepted method to predict γ for bimodal sediments (Bathurst, 2013). Better predictability requires the hiding-exposure effect to be quantified for a comprehensive range of bimodal sand-gravel mixtures under controlled conditions.

1.4. Sediment transport modelling

The adaptation of a single-class approach to a multiple-class approach in sediment transport models has been fundamental for predicting bedload transport of heterogeneous sediments (Amoudry and Souza, 2011). Although the use of this multi-class approach relaxes the assumption that the surficial sediment layer is homogenous, it does not take into account the hiding-exposure effect. Implementation of a hiding-exposure effect in sediment transport models has been shown to better describe the variation in the composition and sorting of sediment across tidal bedforms and sandbanks, and as a result their growth and migration (e.g. Roos et al., 2007a, 2007b; Blondeaux, 2012; Van Oyen et al., 2013). The increased mobility of gravel in a mixture with sand may also help explain the variation in size and preservation potential of sediment waves (Van Landeghem et al., 2009a, 2009b). A better understanding of the hiding-exposure effect is required, including a functional relationship to predict γ against model variables describing the sediment composition and modality, as the use of a constant value of γ was found to lead to a 40–60% error in $\theta_{cr,i}$ estimates (Shvidchenko et al., 2001) which would be amplified due to the nonlinearity of bedload transport rates.

1.5. Aims

The aim of this work is to investigate the hiding-exposure effect for a range of bimodal sand-gravel mixtures representative of coastal and shelf seas. Although the variability of the HE effect has been studied in unimodal and weakly bimodal sediment (e.g. Wilcock, 1993; Shvidchenko et al., 2001; Patel et al., 2013), there is no generally accepted method to predict γ, and therefore ξ_i, for bimodal sediment mixtures (Bathurst, 2013) whilst this is required to accurately represent mixed sediment dynamics in sediment transport models.

Through a comprehensive series of flume experiments, fractional critical Shields parameters, $\theta_{cr,i}$, are determined for different bimodal sand-gravel mixtures. A method is provided to predict γ for bimodal mixtures, which is suitable for implementation in multiple-class sediment transport models. In so doing, the aim is to improve our understanding of fundamental sediment transport processes and their predictability in the natural environment.

2. Methodology

2.1. Coastal and shelf-sea sediment properties

The design of the flume experiments is informed by the observed natural variability of sediment properties in coastal and shelf seas. Sand-gravel mixtures are common in coastal and shelf sea environments globally (Holland and Elmore, 2008) and the Irish Sea is representative of these environments from which a good coverage of sediment samples is available from the British Geological Survey (BGS), Natural Resources Wales (NRW), the Geological Survey of Ireland (GSI) and the Marine Institute (MI) (Fig. 1). The results from particle size analysis of 3187 sediment samples from the Irish Sea were used to inform the sand-gravel flume tank experiments. The non-cohesive sediment considered for this work is characterised by its normalised dry weight fraction of sand, f_s, and gravel, f_g, as shown in Fig. 1b. Pure sand and pure gravel represent 35% of all samples and sand-gravel mixtures represent the remaining 65%. Of the 1330 sediments samples where the modality was available, 58.4% were unimodal, 34.1% were bimodal and the

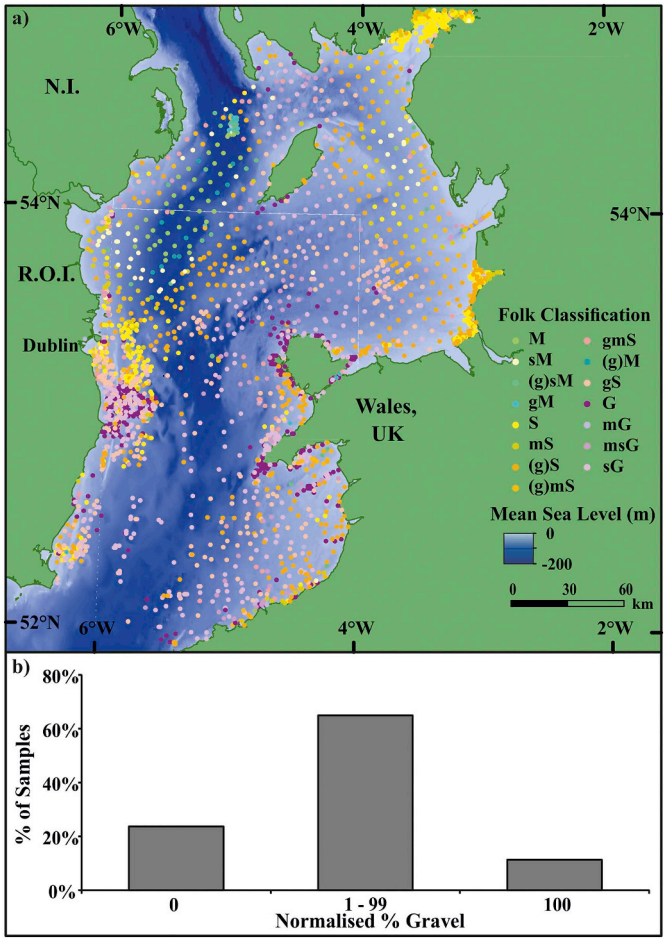

Fig. 1. a) Locations of Irish Sea sediment samples provided by BGS, NRW, GSI and MI, classified according to the Folk classification. The water depth is presented relative to mean sea level (m). b) Normalised percentage of gravel present in the Irish Sea sediment samples.

remaining 7.5% of samples were multimodal. The predominant modes in these samples were medium sand (0.25–0.5 mm) and fine gravel (4–8 mm) with a grain size ratio of 10:1 which is in the same order of magnitude as that seen on the northwest European shelf (Wilson et al., 2018). The flume tank experiments were therefore completed on a range of possible mixtures composed of medium sand and fine gravel. Control experiments were conducted with pure sand and pure gravel.

2.2. Flume experiments

2.2.1. Flume tank setup

The critical shear stress required to entrain sand and gravel fractions in mixtures typical of shelf and coastal seas was quantified through a comprehensive series of laboratory experiments. Experiments were conducted using the vertical recirculating flume in the Hydrodynamics Laboratory at the School of Ocean Sciences, Bangor University. A steady, uniform flow was generated in the flume by a chain-driven propeller connected to an external 4 kW AC motor, capable of producing between 0 and 6000 RPM. The top of the flume includes a transparent, Perspex test section 1.5 m long, 0.20 m wide and 0.14 m deep (Wright and Baas, 2013). Along the base of the test section is an opening (0.14 m wide and 0.30 m long) into which a sample box can be inserted flush with the base of the tank, 1.02 m downstream of where the flow enters the test area (Fig. 2). The sample box was designed in 2 sections: a compartment for the sediment sample (99 mm wide, 150 mm long and 90 mm deep), 75 mm downstream of which was a removable sediment trap (10 mm long and 90 mm deep) with a bed width, *w*, of 99 mm to collect transported material (Fig. 2).

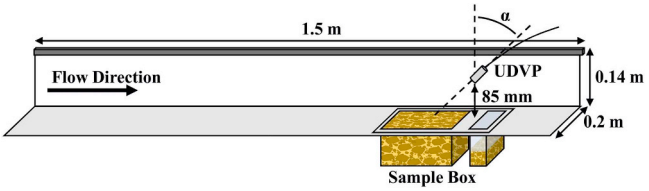

Fig. 2. Schematic diagram of the experimental setup in the test section of the flume tank.

2.2.2. Preparation of sediment mixtures

Predefined sand and gravel mixtures, informed by the observations from the Irish Sea, were prepared using dry weight fractions of sand, f_s, and gravel, f_g, at 5% intervals of f_g from 0 to 50%. The rationale for omitting mixtures containing > 50% gravel (representing 17.5% of the Irish Sea sediment samples) is described in Section 2.2.4. Well-sorted quartz sand with a d_{50} of 0.37 mm and a geometric standard deviation, σ_g, of 1.38 was used in the flume experiments. The gravel was fine and well sorted, with d_{50} = 4.16 mm and σ_g = 1.28. Both the sand and gravel had a density, ρ_s, of 2650 kg m^{-3}. To aid mixing and ease of preparation of the sample bed, freshwater equivalent to 20% of the total dry weight of the sand and gravel was added. The sediment and water were then mixed using an electric hand mixer for 10 mins. Descriptive statistics were generated for the pre-run samples of each mixture via the programme *GRADISTAT v.8* (Blott and Pye, 2001) using the Folk and Ward method (Table 2) and their grain size distributions are shown in Fig. 3. The bimodality index, *B*, and modified bimodality index, B^*, were also calculated for each mixture (Table 2).

Table 2
Descriptive statistics of the sand-gravel mixtures and the exponent γ for each mixture.

f_g	Reps	d_m (mm)	d_{50} (mm)	σ_g	*B*	B^*	γ
0.00	4	0.36	0.37	1.38	0.78	0	0.71
0.05	2	0.36	0.36	1.80	2.61	0.25	0.65
0.10	2	0.36	0.37	1.87	2.65	0.41	0.67
0.15	4	0.68	0.40	2.93	2.67	0.90	0.71
0.20	2	0.75	0.47	2.90	2.21	1.05	0.68
0.25	3	0.78	0.43	3.14	2.57	1.68	0.73
0.30	2	0.77	0.42	3.23	2.72	1.67	0.68
0.35	2	0.78	0.43	3.23	2.71	2.07	0.74
0.40	2	0.82	0.46	3.26	2.66	2.53	0.73
0.45	2	1.40	2.15	3.23	2.58	3.04	0.72
0.50	3	1.65	3.00	3.24	2.98	2.37	0.72
1.00	2	4.05	4.16	1.28	0.91	0	0.86

For each mixture f_g = *fraction of gravel*, *Reps* = *number of replicates*, d_m = *mean grain size*, d_{50} = *median grain size*, σ_g = *sorting*, *B* = *bimodality index (Wilcock, 1993)*, B^* = *modified bimodality index (Sambrook Smith* et al., *1997) and* γ = *the measured exponent in Eq. (19)*, d_m *and* σ_g, *have been calculated using the Folk and Ward Method.*

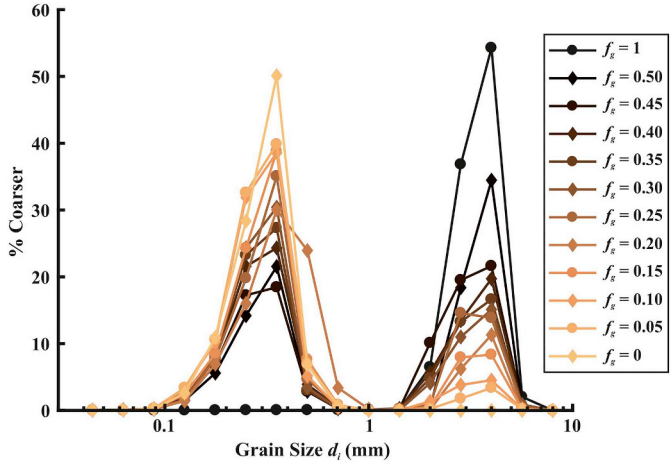

Fig. 3. Grain size distributions of the sand-gravel mixtures.

2.2.3. Experimental procedure

For each mixture, a series of experimental runs were completed with increasing pump frequency (corresponding to bed shear stress): 8 < *F* < 16 Hz for pure sand and the sand-gravel mixtures, and 20 Hz < *F* < 25 Hz for pure gravel. A higher frequency range was used for the pure gravel mixture because of the increased critical shear stress required to mobilise the grains. During each run, a constant water depth, *h*, of 0.13 m above the sediment bed was maintained. At the end of each run, the time, *t*, taken for the sediment trap to fill to a predefined level was recorded and the collection of > 10 g of sediment reduced the errors associated with particle size analysis (the difference in mass before and after sieving) to below 5% loss or gain. This allowed for accurate grain size distribution assessment (Folk and Ward, 1957) via dry sieving at half-phi (*Φ*) intervals from –3*Φ* (8 mm) to 4*Φ* (0.063 mm). The typical sample size was 25 g and the maximum sieving error for all samples was 1.4%. Samples of the post-run bed material were collected for particle size analysis using a core with a diameter of 26 mm to a depth of 15 mm at 3 points along the centre line of the bed. The top layer of the bed was then removed to a depth of 30 mm and replaced before starting the next run at an increased flow velocity to avoid the effects of winnowing from previous runs. The duration of each experimental run was also designed to ensure that transport was not supply-limited. Each set of runs was repeated at least twice to improve the statistical robustness of the results (Table 2).

2.2.4. Determining the shear stresses

Flow velocities were measured using a MET-FLOW ultrasonic Doppler velocimetry profiler (UDVP) with an acoustic frequency of 4 MHz and a diameter of 5 mm. The UDVP was placed in the centre of the flume, 1.4 m downstream of where the flow enters the test section,

at a height, z, of 85 mm above the base of the tank, and orientated at an angle, α, of 45° from vertical to minimise obstruction of the flow and to ensure reflections from the tank walls did not obscure the velocity profiles. The along-beam velocity, v_R, was used to determine the mean horizontal velocity, U, assuming the mean vertical velocity was negligible (i.e. boundary layer assumption):

$$U = \frac{\bar{v}_R}{\sin\alpha}, \tag{12}$$

where the overbar denotes a time average. The UDVP recorded 400 velocity profiles in 60s (sampling rate of 6.7 Hz) and used 178 bins along the beam with a size of 0.74 mm after a blanking distance of 10 mm. This corresponded to a vertical resolution of 0.52 mm for $U(z)$. The bed roughness length, z_0, and the friction velocity, u_*, were calculated using a curve fitting procedure based on the logarithmic law of the wall:

$$U(z) = \frac{u_*}{\kappa}\ln\left(\frac{z}{z_0}\right), \tag{13}$$

where κ is von Kármán's constant taken as 0.41. Curve fitting was applied to the log layer, within the region of $2d_{90} < z < 0.2h$, where d_{90} is the grain size corresponding to the 90th percentile of the grain size distribution for each mixture. Assuming rough turbulent flow, $z_0 = k_s/30$ where k_s is the Nikuradse roughness constrained to be in the range $2d_{50} \le k_s \le 3d_{90}$ such that $d_{50}/12 \le z_0 \le d_{90}/10$ (Fig. 4). It was not necessary to correct for form drag as no bedforms developed during the experiments. The coefficient of determination (R^2) was calculated to assess the fit of the linear regressions. Fig. 4 shows an example of the curve fitting procedure for $F = 10$ Hz and $f_g = 0$. Stagnation of the flow at the transducer is evident in the velocity profile above the maximum velocity. R^2 values ranged between 0.83 and 0.99 for the majority of the fits with one outlier at 0.76. The bed shear stress, τ, was then calculated with Eq. (1), using u_* and $\rho = 998.71$ kg m^{-3}, and was parameterised in terms of the frequency according to

$$\tau = AF^2, \tag{14}$$

where A is a constant which is dependent on f_g in N s^2 m^{-2} with values given in Appendix A. Fig. 5 shows τ versus F^2 for different gravel fractions and the resulting fits according to Eq. (14). For the frequency range, $8 < F < 25$ Hz, the bed shear stress was in the range $0.22 \le \tau \le 8.69$ N m^{-2}. Values of A for mixtures where $f_g = 0.05$, 0.15, 0.25, 0.35 and 0.45 were obtained through linear interpolation.

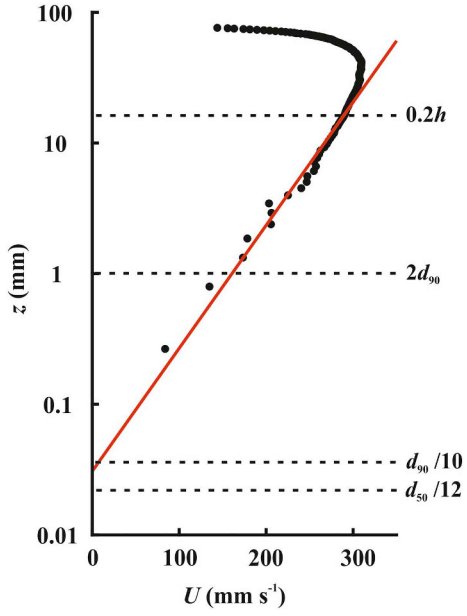

Fig. 4. Example of the logarithmic curve fitting procedure to the velocity profile for $f_g = 0$ and $F = 10$ Hz with z_o constrained between 0.03 and 0.05 mm. The red line is the fitted curve with $R^2 = 0.99$. (For interpretation of the references to colour in this figure legend, the reader is referred to the web version of this article.)

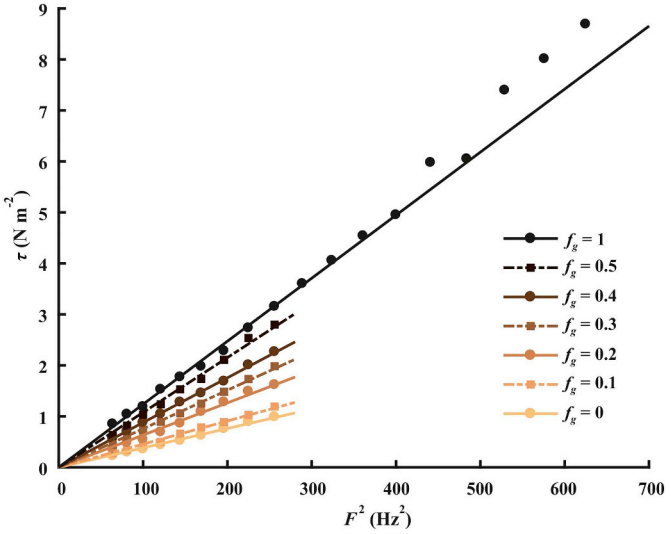

Fig. 5. Parameterisation of the bed shear stress, τ, with the square pump frequency F^2.

The method requires both the gravel and sand fractions to be transported as bedload rather than suspended load. The threshold of suspension for sediment is given by $w_s \sim u_*$, where w_s is the settling velocity, such that the minimum stress, τ_{min}, required for suspension is

$$\tau_{min} = \rho w_s^2. \tag{15}$$

According to Soulsby (1997), $w_s = 0.056$ m s^{-1} and $\tau_{min} = 3.13$ N m^{-2} for the sand fraction used herein. The suspension criterion of the sand fraction would be met with $F > 17$ Hz and for all sand-gravel mixtures with $f_g > 0.5$. Thus, to limit sediment transport to bedload only, F was constrained to $8 \le F \le 16$ Hz for $f_g \le 0.5$, and sand-gravel mixtures with $f_g > 0.5$ were omitted. To mobilise the pure gravel as bedload, F in the range $20 \le F \le 25$ Hz was required.

2.2.5. Calculating the critical shear stress of size fractions

To determine the critical Shields parameter of the sand and gravel fractions, the Parker et al. (1982) reference transport method adapted by Shvidchenko et al. (2001) was used. This method relates $\theta_{cr,i}$ to $q_{b,i}^*$, normalised by the proportion of the transported grain size fraction in the bed surface material, f_i:

$$q_{b,i}^* = \frac{q_{b,i}}{f_i\sqrt{(s-1)gd_i^3}}, \tag{16}$$

where $q_{b,i}$, the volume transport rate of sediment (excluding voids), was calculated using the formula of Gaweesh and Van Rijn (1994):

$$q_{b,i} = \frac{M_i}{\rho_s wt}, \tag{17}$$

where M_i is the mass of each i^{th} grain size fraction retained in sieves, w is the bed width of the sediment trap (99 mm) and t is the time taken for the trap to fill to the predefined level. The volumetric bedload transport rate, q_b, is then equivalent to:

$$q_b = \sum_{i=1}^{n} q_{b,i}. \tag{18}$$

Least squares regression was used to extrapolate values of $\theta_{cr,i}$, taken as the θ_i value at a reference transport rate of $q_{b,i}^* = 10^{-4}$ for each

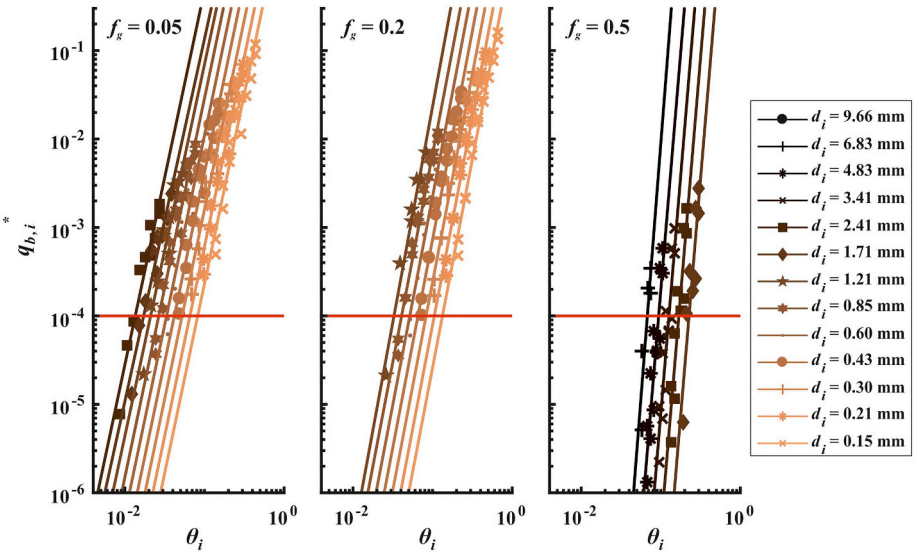

Fig. 6. Log-log plots of the fractional Shields parameter, θ_i, and dimensionless bedload transport rate, $q_{b,i}^*$, for mixtures of f_g = 0.05, 0.2 and 0.5. The reference transport rate of $q_{b,i}^* = 10^{-4}$ is shown by the red line. (For interpretation of the references to colour in this figure legend, the reader is referred to the web version of this article.)

grain size fraction thus approximating the lower limit of bedload transport that can be accurately measured in laboratory experiments (Shvidchenko et al., 2001).

3. Results

A total of 281 experiments were completed with a duration of 337 h. For individual experiments, t ranged from 69 s to 25 h. Volumetric bedload transport rates, q_b, ranged between $0.06 \times 10^{-9}\,m^2\,s^{-1}$ and $0.18 \times 10^{-6}\,m^2\,s^{-1}$. To calculate $\theta_{cr,i}$, M_i and f_i were obtained through particle size analysis of the transported material and the pre-run bed material, respectively. M_i was then used to calculate $q_{b,i}$ with Eq. (17). Values of τ, f_i, and $q_{b,i}$ were used to calculate θ_i and $q_{b,i}^*$ with Eqs. (5a) and (16) respectively. Log-log plots of θ_i vs $q_{b,i}^*$ were then produced for each mixture, and least squares regression was used to extrapolate values of θ_i at $q_{b,i}^* = 10^{-4}$, taken as $\theta_{cr,i}$ (Fig. 6). Fig. 6 shows that $\theta_{cr,i}$ increases as f_g was increased. This variation of $\theta_{cr,i}$ with f_g between mixtures for individual grain sizes is further explored in Fig. 7a. Within mixtures, $\theta_{cr,i}$ decreases (Fig. 7a) and $\tau_{cr,i}$ increases (Fig. 7b) with increasing d_i. Pure sand with d_i = 0.15 mm requires a shear stress of 0.20 N m^{-2} to become mobile compared with 0.95 N m^{-2} for a sand-gravel mixture with f_g = 0.5, which is equivalent to a 75% increase in $\tau_{cr,i}$. Pure gravel with d_i = 2.41 mm requires $\tau_{cr,i}$ = 6.59 N m^{-2} to become mobile whereas for a sand-gravel mixture with f_g = 0.5, $\tau_{cr,i}$ = 2.14 N m^{-2}, which is equivalent to a 64% decrease in $\tau_{cr,i}$.

3.1. Calculating the hiding-exposure effect in the sand-gravel mixtures

In Fig. 8, $\theta_{cr,i}/\theta_{cr,50}$ is plotted against d_i/d_{50}, and the formula of Egiazaroff (1965), Ashida and Michiue (1973), and Wilcock and Crowe (2003) are included for comparison. The data show a dependency of $\theta_{cr,i}/\theta_{cr,50}$ on f_g, illustrated with an increase in $\theta_{cr,i}/\theta_{cr,50}$ for $d_i/d_{50} < 1$ and a decrease in $\theta_{cr,i}/\theta_{cr,50}$ for $d_i/d_{50} > 1$ with increasing f_g. The formula of Egiazaroff (1965) is shown to be representative only for $0.4 < d_i/d_{50} < 1$, and it overpredicts $\theta_{cr,i}/\theta_{cr,50}$ by up to a factor of 13 for $d_i/d_{50} = 0.07$, below which the formula is not valid. The formula of Ashida and Michiue (1973) is more accurate in that it overpredicts values of $\theta_{cr,i}/\theta_{cr,50}$ by a factor of 2–4 for $d_i/d_{50} < 0.2$ and it is valid below $d_i/d_{50} = 0.07$. As this formula is an adaptation of Egiazaroff's (1965) formula, it too overpredicts $\theta_{cr,i}/\theta_{cr,50}$ for $d_i/d_{50} > 1$. The formula of Wilcock and Crowe (2003) is the most accurate for $d_i/d_{50} < 1$, closely matching the curve fitted to the pure gravel data. It too, however, overpredicts $\theta_{cr,i}/\theta_{cr,50}$ for $d_i/d_{50} > 1$. For each mixture, the

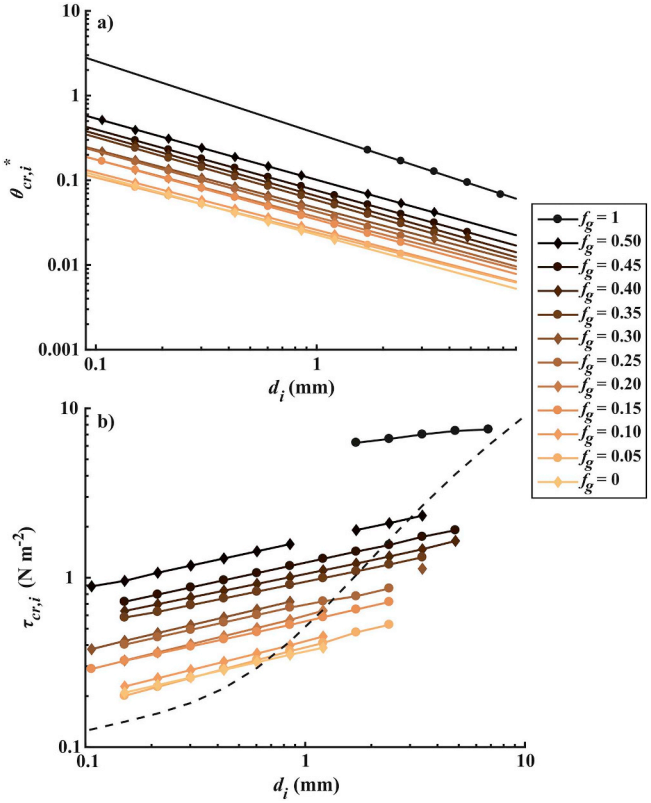

Fig. 7. a) Extrapolated $\theta_{cr,i}$ values plotted against d_i for each mixture. b) Equivalent $\tau_{cr,i}$ values, calculated using an average water density of 998.71 kg m^{-3}, vs d_i. Values of $\tau_{cr,i}$ equivalent to the Shields curve are shown with the dashed black line.

relationship between $\theta_{cr,i}/\theta_{cr,50}$ and d_i/d_{50} was investigated further by fitting power curves to the data of the form:

$$\xi_i = \left(\frac{d_i}{d_{50}}\right)^{-\gamma}. \tag{19}$$

For all mixtures, the exponent γ generally increased with increasing f_g from 0.65 to 0.86 (Fig. 9d and Table 2). In Fig. 9a, b and c, γ is plotted

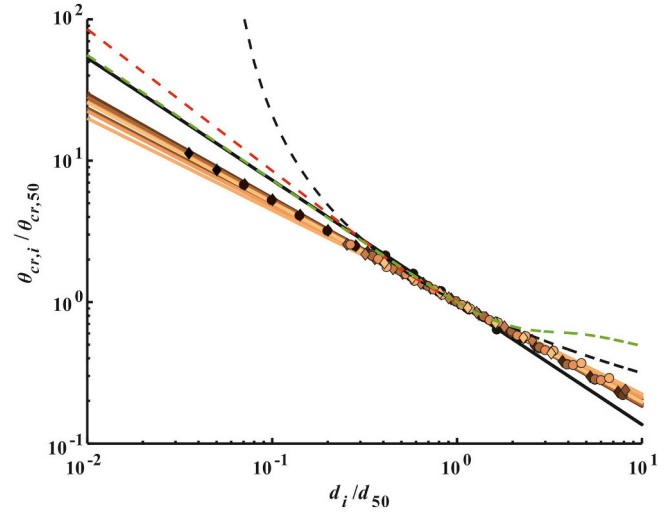

Fig. 8. $\theta_{cr,i}/\theta_{cr,50}$ vs d_i/d_{50} for each mixture using the same symbology as Fig. 7, edged in black for clarity. The HE formulae of Egiazaroff (1965), Ashida and Michiue (1973), and Wilcock and Crowe (2003) are shown as dashed black, red and green lines, respectively. (For interpretation of the references to colour in this figure legend, the reader is referred to the web version of this article.)

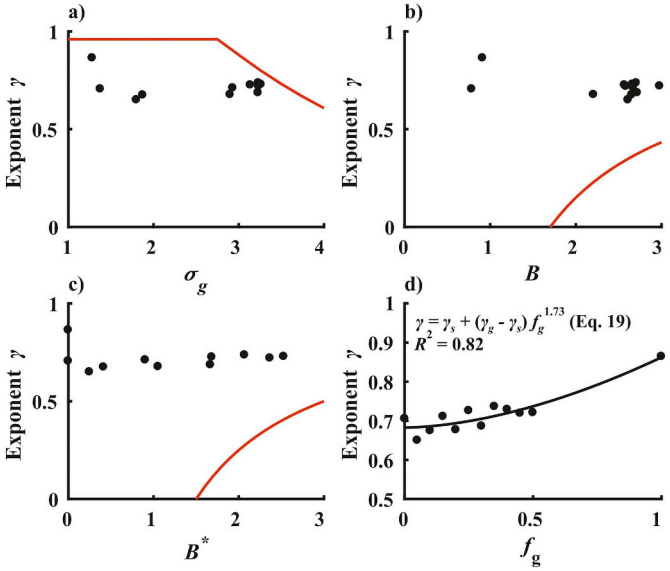

Fig. 9. Plots of γ against a) σ_g, b) B, c) B^* and d) f_g. The red lines show the values of γ using the predictors of: a) Patel et al. (2013) with σ_g; b) Wilcock (1993) with B; and c) that modified for B^* by Patel et al. (2013). (For interpretation of the references to colour in this figure legend, the reader is referred to the web version of this article.)

against the geometric standard deviation, σ_g, the bimodality index, B, and the modified bimodality index, B^*, for the mixtures used herein. The use of B better describes the bimodality of sediment mixtures than B^* (Fig. 9b and c, and Table 2). The $B < 1.7$ definition only includes the pure sand and gravel cases, whereas the $B^* < 1.5$ definition includes mixtures where $0.05 \leq f_g \leq 0.2$ (which are clearly bimodal, Fig. 3) as well as the pure sand and gravel cases. Predicted values of γ using the formulae of Wilcock (1993) and Patel et al. (2013) for σ_g, B and B^*, respectively, are also shown in Fig. 9a, b, and c. The dependence of γ on f_g is plotted in Fig. 9d. There is no relationship between γ and σ_g, and it does not fit the relationship proposed by Patel et al. (2013) (Eq. (11)). The exponent γ remains constant with B and increases slightly, in a non-linear way, with B^* except for the pure sand and gravel (Fig. 9b and c). The formulae of Wilcock (1993) and Patel et al. (2013) both underestimate γ for the sand-gravel mixtures (Fig. 9b and c). There is, however, a statistically significant non-linear relationship between γ and f_g (Fig. 9d) for which the best fit is given by a two-term power function with $R^2 = 0.82$ ($p < 0.05$):

$$\gamma = \gamma_s + (\gamma_g - \gamma_s) f_g^{1.73}, \tag{20}$$

where the exponent for pure sand, γ_s, obtained from this correlation is 0.68, and that for pure gravel, γ_g, is 0.86. With the pure gravel case excluded R^2 decreases to 0.38 ($p < 0.05$) and the f_g coefficient and power drop from 0.18 and 1.73 to 0.12 and 1.2, but the trend in the data remains the same and is statistically significant.

4. Discussion

4.1. Interpretation of the results

The presence and strength of the HE effect is evident here initially through the need for higher bed shear stresses to mobilise pure gravel which, when mixed with sand, became mobile at much lower bed shear stresses. The HE effect for the bimodal sand-gravel mixtures used herein resulted in an increase in $\tau_{cr,i}$ by up to 75% for sand sized fractions ($d_i = 0.15$ mm) and a decrease in $\tau_{cr,i}$ by up to 64% for gravel sized fractions ($d_i = 2.41$ mm). This is equivalent to a variation in the threshold of motion by up to a factor of 3 for grain sizes in the range of $0.03 < d_i/d_{50} < 1$. The HE correction, ξ_i, i.e. the relationship between the $\theta_{cr,i}/\theta_{cr,50}$ and d_i/d_{50}, presented in Eq. (19), is similar to that presented in other studies (e.g. Parker et al., 1982; Wilcock and Crowe, 2003) in that it follows a power law relationship. Previously, there has been some success in relating γ to d_{50} and σ_g for unimodal and weakly bimodal mixtures, and to B or B^* for bimodal mixtures (e.g. Misri et al., 1984; Wilcock, 1993; Shvidchenko et al., 2001; Patel et al., 2013). Currently, however, only the formulae of Shvidchenko et al. (2001) and Patel et al. (2013) which relate γ to σ_g are applicable to both unimodal and bimodal sediment. Although σ_g provides a description of the shape of a grain size distribution for unimodal sediment, its applicability to bimodal sediments is unclear. This study confirms that doubt, as no clear relationship between γ and σ_g was observed (Fig. 9a). The relationship between γ and σ_g proposed by Patel et al. (2013) overpredicts γ (Fig. 9a). When testing the relationship between γ and the more appropriate parameter B or B^* for bimodal sediment mixtures (Wilcock, 1993; Patel et al., 2013), the existing relationships under predict γ for the sand-gravel mixtures in this study and γ appears to remain constant when plotted against B or B^* (Fig. 9b and c). Although the use of a constant γ is advocated in other studies (e.g. Buffington and Montgomery, 1997), the small variation in γ identified in this study can have a significant effect on the critical shear stress, $\tau_{cr,i}$, for individual grain size classes in a mixture compared with uniform sediment of a similar size (Fig. 7b). When using a constant value of γ, the variability in mobility of different fractions in mixed sediments will, therefore, be lost. Here, a significant dependence of γ, and therefore ξ_i, on the proportion of gravel, f_g, to sand, f_s, in a mixture has been identified (Fig. 9d). This relationship is described by Eq. (20) which is constrained by the exponent for the pure sand, $\gamma_s = 0.68$, and that for the pure gravel, $\gamma_g = 0.86$. The fact that γ_g is larger than γ_s is consistent with the strong dependence of γ on the d_{50} of a mixture primarily as identified by Shvidchenko et al. (2001) (Eq. (8)). The values of γ_s and γ_g calculated using this relationship (0.55 and 1.17 respectively) are different for potentially a number or reasons: 1) γ controls the variation in HE only for grains where $d_i/d_{50} < 1$ whereas the γ in our experiments controls the variation for the complete grain size range; 2) Shvidchenko et al.'s (2001) relationship is based not only on unimodal mixtures; and 3) in the case of γ_s, the grain size is outside Shvidchenko et al.'s (2001) range of applicability.

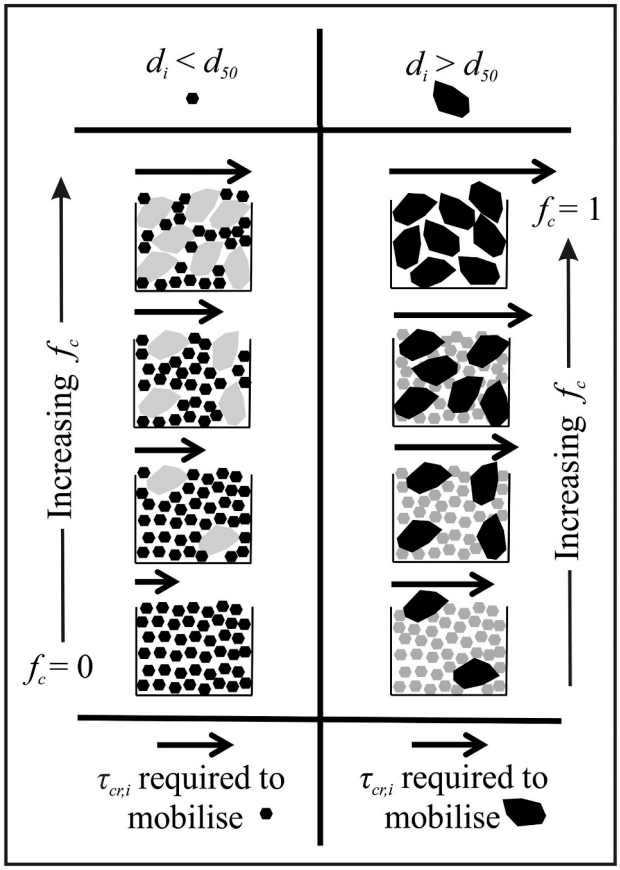

Fig. 10. Schematic diagram illustrating the variation in the hiding-exposure effect, ξ_i, and the exponent, γ, for a fine grain ($d_i < d_{50}$) and a coarse grain ($d_i > d_{50}$) in sediment mixtures with varying fractions of coarse material, f_c.

It is proposed that with an increased proportion of coarse to fine material, the probability of coarse grains being exposed to the flow, and therefore fine grains being hidden from the flow, increases, thus increasing the strength of the HE effect and as a result γ. This process is represented schematically in Fig. 10. Coarse sediment, in a unimodal mixture, requires a high critical shear stress to be mobilised, whilst the fine unimodal sediment is readily mobile at a low critical shear stress. When coarse sediment is mixed with fine sediment, the critical shear stress to mobilise the coarse sediment decreases due to exposure effects, whilst the hiding effect renders the fine fraction more difficult to mobilise. For a certain mixture of fine and coarse sediments, the exposure effect on the coarse fraction and the hiding effect on fine fraction is such that both sediment fractions require the same critical shear stress to be mobilised ($\gamma = 1$).

4.2. Implications for sediment transport modelling

It is evident from the results that the presence of mixed sand-gravel, common across glaciated shelf seas, coastal and riverine environments (Holland and Elmore, 2008), can greatly affect the mobility of individual grain size fractions. Bedload transport rate predictions using single-class models have been shown to lie within a factor of 5 of measured values for simple cases (currents alone) and lie within a factor of > 10 for complex cases (waves alone and combined waves and currents) (Soulsby and Damgaard, 2005), and this uncertainty is greatest in the presence of mixed sediments (Wilson et al., 2018). Despite a move from single-class to multiple-class sediment transport models (Warner et al., 2008b; Amoudry and Souza, 2011), the use of fixed $\theta_{cr,i}$ values does not account for intergranular effects and models which employ a HE correction typically use that of Egiazaroff (1965) or its adapted form (Ashida and Michiue, 1972), which only seem valid for $0.4 < d_i/d_{50} < 1$ (e.g. Komar, 1987). The HE formula presented here applies to bimodal sediments and provides a relationship for γ, and therefore ξ_i, which can be estimated for a wide range of mixtures. Importantly, using Eq. (20) does not relate γ to quantities that are difficult to implement in multiclass numerical models, such as σ_g. Eq. (20) also maintains the dependence of γ on d_{50} in that it does not constrain γ to the same/similar value(s) for pure sand and pure gravel, as a relationship to B or B* would. Instead, f_g often is an easily available model variable in multiclass numerical models (e.g., Warner et al., 2008b), which is dynamically computed, thus enabling changes in surficial bed properties to be accounted for after erosion and deposition cycles.

5. Conclusions

In this work, the effect that bimodal sediment mixtures have on the threshold of motion of individual grain sizes due to the hiding-exposure effect has been demonstrated. The Irish Sea is used here as a test bed, but the results are thought to be extendable to larger shelf seas such as the north-west European shelf. The mobility of fine sediment decreases by up to 75% and the mobility of coarse sediment increases by up to 64%. This is dependent on the ratio of the coarsest mode to the finest mode in a sediment mixture. The mobility of seabed sediments and associated bed forms can have important implications for sediment extraction and consumers of shelf sea resources as well as coastal zone managers. Therefore, to fully understand bedload transport processes at these small scales, there is a need to account for mixed sediment dynamics when modelling sediment transport pathways. A hiding-exposure effect is presented here to account for the effects of mixed sediment dynamics which:

1. Includes for variations in the mobility of not only the fine fractions ($d_i/d_{50} < 1$) but also for coarse fractions ($d_i/d_{50} > 1$) in fully bimodal sediment mixtures.
2. Is dynamic, in that the strength of the HE effect changes with the composition of the seabed sediment due to deposition/erosion by varying γ rather than using a fixed value.
3. Provides a less computationally expensive method of predicting γ for sediment mixtures by using f_g to describe the mixture composition compared with previous methods where γ is related to d_{50} and σ_g.
4. Is applicable to coastal and shelf seas where the composition of seabed sediments is a result of the reworking of glacial/fluvial deposits by contemporary hydrodynamic regimes.

Acknowledgments

Funding was provided by the Natural Environment Research Council (NERC) with CJMcC's studentship through the ENVISION Doctoral Training Partnership. KJJVL acknowledges the financial support provided by the Welsh Government and Higher Education Funding Council for Wales through the Sêr Cymru National Research Network for Low Carbon, Energy, and Environment. LOA wishes to acknowledge NERC funding via grant NE/N015894/1 and national capability funding to NOC. JM acknowledges support from a European Research Council Consolidator Award (725955). The authors are grateful for access to seabed sediment sample data made available by the British Geological Survey (BGS), the Geological Survey of Ireland (GSI),the Marine Institute (MI) and Natural Resources Wales (NRW). Thanks are also extended to Nathan Howard and Nicolas Ducharneux for their assistance in the flume laboratory, and to Mallory Diggens for her insightful advice.

Notation

Symbol	Description	Units
B	Bimodality Index	-
B^*	Modified Bimodality Index	-
d_i	Grain size of the i^{th} fraction	m
d_c	Grain size of the coarse mode in Eq. (9a)	m
d_f	Grain size of the fine mode in Eq. (9a)	m
d_{50}	Median grain size	m
d_{90}	90th Percentile Grain Size	m
d_m	Mean grain size	m
d_n	Representative grain size (d_m or d_{50})	m
d_i/d_{50}	Relative grain size	-
f_i	Proportion of the i^{th} fraction in the bed material	-
f_c	Fraction of the coarse mode in Eq. (9a)	-
f_f	Fraction of the fine mode in Eq. (9a)	-
f_1	Fraction of the primary mode in Eq. (9b)	-
f_2	Fraction of the secondary mode in Eq. (9b)	-
f_s	Dry weight fraction of sand	-
f_g	Dry weight fraction of gravel	-
F	Pump Frequency	Hz
g	Acceleration due to gravity	m s^{-2}
h	Depth of water column	m
k_s	Nikuradse Roughness	m
l	log(d_{50}) in Eq. (8)	-
M_i	Mass of i^{th} fraction retained on sieves	kg
n	Constant in hiding-exposure formulae	-
q_b^*	Einstein bedload parameter	-
$q_{b,i}^*$	Einstein bedload parameter for the i^{th} fraction	-
q_b	Volumetric transport rate per unit bed width	m^2 s^{-1}
$q_{b,i}$	Volumetric transport rate of the i^{th} fraction	m^2 s^{-1}
$s = \rho_s/\rho$	Specific density of sediment	-
t	Experiment Duration	s
u_*	Friction velocity	m s^{-1}
U	Temporal mean horizontal flow velocity	m s^{-1}
$\bar{v}_R$	Temporal mean along-beam flow velocity	m s^{-1}
w	Bed width	m
w_s	Settling velocity	m s^{-1}
z	Height above the bed	m
z_0	Roughness length	m
α	Transducer Angle	°
γ	Exponent in equation Eq. (20)	-
θ	Shields parameter	-
θ_i	Shields parameter for the i^{th} fraction	-
θ_{cr}	Critical Shields parameter	-
$\theta_{cr,i}$	Critical Shields parameter for the i^{th} fraction	-
$\theta_{cr,50}$	Critical Shields parameter for the median grain size	-
κ	von Kármán's constant	-
$\xi_i = \theta_{cr,i}/\theta_{cr,50}$	Hiding-exposure correction for the i^{th} fraction	-
ρ	Density of water	kg m^{-3}
ρ_s	Density of sediment	kg m^{-3}
$\sigma_g = (d_{84}/d_{16})^{1/2}$	Grain size sorting (geometric standard deviation)	-
τ	Bed shear stress	N m^{-2}
τ_i	Bed shear stress of the i^{th} fraction	N m^{-2}
τ_{cr}	Critical shear stress	N m^{-2}
$\tau_{cr,i}$	Critical shear stress of the i^{th} fraction	N m^{-2}
$\tau_{cr,50}$	Critical shear stress of the median grain size	N m^{-2}
τ_{min}	Minimum stress required for suspension	N m^{-2}
Φ_1	Grain size of the primary mode in Eq. (9b)	Φ-units
Φ_2	Grain size of the secondary mode in Eq. (9b)	Φ-units

Appendix A. Values of A for each mixture

f_g	A (N s^2 m^{-2})
0.00	0.0038
0.10	0.0045
0.20	0.0063
0.30	0.0076
0.40	0.0088
0.50	0.0108
1.00	0.0124

References

Aliotta, S., Perillo, G.M.., 1987. A sand wave field in the entrance to Bahia Blanca Estuary, Argentina. Mar. Geol. 76, 1–14.

Amoudry, L.O., Souza, A.J., 2011. Deterministic coastal morphological and sediment transport modeling: a review and discussion. Rev. Geophys. 49, RG2002. https://doi.org/10.1029/2010RG000341.

Ashida, K., Michiue, M., 1971. An investigation of river bed degradation downstream of a dam. In: Proc. of 14th IAHR Congress. Wallingford, U.K. pp. 1–9.

Ashida, K., Michiue, M., 1972. Study on hydraulic resistance and bed-load transport rate in alluvial streams. Proc. Jpn Soc. Civ. Eng. 1972, 59–69.

Ashida, K., Michiue, M., 1973. Study on bed load transport rate in open channel flows. In: International Symposium on River Mechanics, pp. 1–12.

Bagnold, R.A., 1956. The flow of cohesionless grains in fluids. Philos. Trans. R. Soc. A Math. Phys. Eng. Sci. 249, 235–297.

Bagnold, R.A., 1966. An approach to the sediment transport problem from general physics. US Geological Survey Professional Paper, Washington.

Bathurst, J.C., 2013. Critical conditions for particle motion in coarse bed materials of nonuniform size distribution. Geomorphology 197, 170–184.

Blondeaux, P., 2012. Sediment mixtures, coastal bedforms and grain sorting phenomena: an overview of the theoretical analyses. Adv. Water Resour. 48, 113–124.

Blott, S.J., Pye, K., 2001. GRADISTAT: a grain size distribution and statistics package for the analysis of unconsolidated sediments. Earth Surf. Process. Landf. 26, 1237–1248.

Buffington, J.M., Montgomery, D.R., 1997. A systematic analysis of eight decades of incipient motion studies, with special reference to gravel-bedded rivers. Water Resour. Res. 33, 1993–2029.

Buffington, J.M., Montgomery, D.R., 1998. Correction to "a systematic analysis of eight decades of incipient motion studies, with special reference to gravel-bedded rivers.". Water Resour. Res. 34 (157–157).

Diesing, M., Stephens, D., Aldridge, J., 2013. A proposed method for assessing the extent of the seabed significantly affected by demersal fishing in the Greater North Sea. ICES J. Mar. Sci. 70, 1085–1096.

Diesing, M., Kröger, S., Parker, R., Jenkins, C., Mason, C., Weston, K., 2017. Predicting the standing stock of organic carbon in surface sediments of the north–west European continental shelf. Biogeochemistry 135, 183–200.

Egiazaroff, I.V., 1965. Calculation of non-uniform sediment concentrations. J. Hydraul. Div. ASCE 91, 225–247.

Einstein, H.A., 1950. The bed-load function for sediment transportation in open channel flows. In: Technical Bulletin 1026. United States Department of Agriculture, Soil Conservation Service, Washington, DC.

Engelund, F., Fredsøe, J., 1976. A sediment transport model for straight alluvial channels. Hydrol. Res. 7, 293–306.

Engelund, F., Hansen, E., 1967. A Monograph on Sediment Transport in Alluvial Streams. Technical Press, Copenhagen.

Folk, R., Ward, W., 1957. Brazos River bar: a study in the significance of grain size parameters. J. Sediment. Petrol. (27), 3–26.

Gaweesh, M.T.K., van Rijn, L.C., 1994. Bed-load sampling in sand-bed rivers. J. Hydraul. Eng. 120, 1364–1384.

Hayashi, T.S., Ozaki, Ichibashi, T., 1980. Study on the bed load transport of sediment mixture. In: Proceedings of the Japanese Conference on Hydraulics. 24. pp. 35–43.

Hiddink, J.G., Jennings, S., Sciberras, M., Szostek, C.L., Hughes, K.M., Ellis, N., Rijnsdorp, A.D., McConnaughey, R.A., Mazor, T., Hilborn, R., Collie, J.S., Pitcher, C.R., Amoroso, R.O., Parma, A.M., Suuronen, P., Kaiser, M.J., 2017. Global analysis of depletion and recovery of seabed biota after bottom trawling disturbance. Proc. Natl. Acad. Sci. 114, 8301–8306.

Holland, K.T., Elmore, P.A., 2008. A review of heterogeneous sediments in coastal environments. Earth Sci. Rev. 89, 116–134.

James, I., 2002. Modelling pollution dispersion, the ecosystem and water quality in coastal waters: a review. Environ. Model. Softw. 17, 363–385.

Kleinhans, M.G., van Rijn, L.C., 2002. Stochastic prediction of sediment transport in sand-gravel bed rivers. J. Hydraul. Eng. 128, 412–425.

Knaapen, M.A.F., Hulscher, S.J.M.H., 2002. Regeneration of sand waves after dredging. Coast. Eng. 46, 277–289.

Komar, P.D., 1987. Selective grain entrainment by a current from a bed of mixed sizes: a reanalysis. J. Sediment. Petrol. 57, 203–211.

Kuhnle, R.A., 1992. Fractional transport rates of bedload on Goodwin Creek. In: Billi, P., Hey, R.D., Thorne, C.R. (Eds.), Dynamics of Gravel-bed Rivers, pp. 141–155.
Kuhnle, R.A., 1993a. Fluvial transport of sand and gravel mixtures with bimodal size distributions. Sediment. Geol. 85, 17–24.
Kuhnle, R.A., 1993b. Incipient motion of sand-gravel sediment mixtures. J. Hydraul. Eng. 119, 1400–1415.
Le Bot, S., Lafite, R., Fournier, M., Baltzer, A., Desprez, M., 2010. Morphological and sedimentary impacts and recovery on a mixed sandy to pebbly seabed exposed to marine aggregate extraction (Eastern English Channel, France). Estuar. Coast. Shelf Sci. 89, 221–233.
Lesser, G.R., Roelvink, J.A., van Kester, J.A.T.M., Stelling, G.S., 2004. Development and validation of a three-dimensional morphological model. Coast. Eng. 51, 883–915.
Ling, S.D., Sinclair, M., Levi, C.J., Reeves, S.E., Edgar, G.J., 2017. Ubiquity of micro-plastics in coastal seafloor sediments. Mar. Pollut. Bull. 121, 104–110.
Malham, S.K., Rajko-Nenow, P., Howlett, E., Tuson, K.E., Perkins, T.L., Pallett, D.W., Wang, H., Jago, C.F., Jones, D.L., McDonald, J.E., 2014. The interaction of human microbial pathogens, particulate material and nutrients in estuarine environments and their impacts on recreational and shellfish waters. Environ. Sci.: Processes Impacts 16, 2145–2155.
Meyer-Peter, E., Müller, R., 1948. Formulas for bed-load transport. In: Proceedings of the 2nd Meeting of the International Association of Hydraulic Structures Research, pp. 39–64.
Misri, R.L., Garde, R.J., Ranga Raju, K.G., 1984. Bed load transport of coarse nonuniform sediment. J. Hydraul. Eng. 110, 312–328.
Nielsen, P., 1992. Coastal Bottom Boundary Layers and Sediment Transport. Advanced Series on Ocean Engineering.
Parker, G., Klingeman, P.C., McLean, D.G., 1982. Bedload and size distribution in paved gravel-bed streams. J. Hydraul. Div. 108, 544–571.
Patel, S.B., Patel, P.L., Porey, P.D., 2013. Threshold for initiation of motion of unimodal and bimodal sediments. Int. J. Sediment Res. 28, 24–33.
Redding, J.H., 2000. Experimental manipulation of sandwaves to reduce their navigation hazard potential, Jade shipping channel, N. Germany. In: Proceedings of the 1st International Conference Workshop on Marine Sandwave Dynamics. University of Lille, pp. 169–176.
Roos, P.C., Hulscher, S.J.M.H., Van der Meer, F., Wientjes, I.G.M., 2007a. Grain size sorting over offshore sandwaves: Observations and modelling. In: Dohmen-Janssen, C.M., Hulscher, S.J.M.H (Eds.), River, Coastal and Estuarine Morphodynamics, RCEM 2007, 17-21 September 2007, Enschede, The Netherlands. I. Taylor & Francis, London, pp. 649–656.
Roos, P.C., Wemmenhove, R., Hulscher, S.J.M.H., Hoeijmakers, H.W.M., Kruyt, N.P., 2007b. Modeling the effect of nonuniform sediment on the dynamics of offshore tidal sandbanks. J. Geophys. Res. 112, F02011. https://doi.org/10.1029/2005JF000376.
Sambrook Smith, G.H., Nicholas, A.P., Ferguson, R.I., Smith, G.H.S., Nicholas, A.P., Ferguson, R.I., 1997. Measuring and defining bimodal sediments: problems and implications. Water Resour. Res. 33, 1179–1185.
Shields, A., 1936. Application of similarity principles and turbulence research to bed-load movement. In: Mitt. Preuss. Versuchsanst. Wasserbau Schiffbau. 26. pp. 47.
Shvidchenko, A.B., Pender, G., Hoey, T.B., 2001. Critical shear stress for incipient motion of sand/gravel streambeds. Water Resour. Res. 37, 2273–2283.
Snelgrove, P.V.R., Soetaert, K., Solan, M., Thrush, S., Wei, C.-L., Danovaro, R., Fulweiler, R.W., Kitazato, H., Ingole, B., Norkko, A., Parkes, R.J., Volkenborn, N., 2018. Global carbon cycling on a heterogeneous seafloor. Trends Ecol. Evol. 33, 96–105.
Soulsby, R., 1997. Dynamics of Marine Sands. A Manual for Practical Applications. Thomas Telford Services Ltd., London.
Soulsby, R.L., Damgaard, J.S., 2005. Bedload sediment transport in coastal waters. Coast. Eng. 52, 673–689.
Stephens, D., Diesing, M., 2015. Towards quantitative spatial models of seabed sediment composition. PLoS One 10, e0142502. https://doi.org/10.1371/journal.pone.0142502.
Sumer, B.M., Whitehouse, R.J., Tørum, A., 2001. Scour around coastal structures: a summary of recent research. Coast. Eng. 44, 153–190.
Van Lancker, V.R.M., Bonne, W., Garel, E., Degrendele, K., Roche, M., Van den Eynde, D., Bellec, V., Briere, C., Collins, M.B., Velegrakis, A.F., 2010. Recommendations for the sustainable exploitation of tidal sandbanks. J. Coast. Res. Spec. Issue (51), 151–164.
Van Landeghem, K.J.J., Uehara, K., Wheeler, A.J., Mitchell, N.C., Scourse, J.D., 2009a. Post-glacial sediment dynamics in the Irish Sea and sediment wave morphology: data–model comparisons. Cont. Shelf Res. 29, 1723–1736.
Van Landeghem, K.J.J., Wheeler, A.J., Mitchell, N.C., Sutton, G., 2009b. Variations in sediment wave dimensions across the tidally dominated Irish Sea, NW Europe. Mar. Geol. 263, 108–119.
Van Oyen, T., Blondeaux, P., Van den Eynde, D., 2013. Sediment sorting along tidal sand waves: a comparison between field observations and theoretical predictions. Cont. Shelf Res. 63, 23–33.
van Rijn, L.C., 1984. Sediment transport, part I: bed load transport. J. Hydraul. Eng. 110, 1431–1456.
van Rijn, L.C., 2007. Unified view of sediment transport by currents and waves. III: graded beds. J. Hydraul. Eng. 133, 761–775.
Ward, S.L., Neill, S.P., Van Landeghem, K.J.J., Scourse, J.D., 2015. Classifying seabed sediment type using simulated tidal-induced bed shear stress. Mar. Geol. 367, 94–104.
Warner, J.C., Butman, B., Dalyander, P.S., 2008a. Storm-driven sediment transport in Massachusetts Bay. Cont. Shelf Res. 28, 257–282.
Warner, J.C., Sherwood, C.R., Signell, R.P., Harris, C.K., Arango, H.G., 2008b. Development of a three-dimensional, regional, coupled wave, current, and sediment-transport model. Comput. Geosci. 34, 1284–1306.
Wienberg, C., Hebbeln, D., 2005. Impact of dumped sediments on subaqueous dunes, outer Weser Estuary, German Bight, southeastern North Sea. Geo-Mar. Lett. 25, 43–53.
Wilcock, P.R., 1993. Critical shear stress of natural sediments. J. Hydraul. Eng. 119, 491–505.
Wilcock, P.R., 2001. Toward a practical method for estimating sediment-transport rates in gravel-bed rivers. Earth Surf. Process. Landf. 26, 1395–1408.
Wilcock, P.R., Crowe, J.C., 2003. Surface-based transport model for mixed-size sediment. J. Hydraul. Eng. https://doi.org/10.1061/(ASCE)0733-9429(2003)129:2(120).
Wilcock, P.R., Kenworthy, S.T., 2002. A two-fraction model for the transport of sand/gravel mixtures. Water Resour. Res. https://doi.org/10.1029/2001WR000684.
Wilson, R.J., Speirs, D.C., Sabatino, A., Heath, M.R., 2018. A synthetic map of the north-west European Shelf sedimentary environment for applications in marine science. Earth Syst. Sci. Data 10, 109–130.
Wright, J.D., Baas, J.H., 2013. Despiking ultrasonic doppler velocity-profiling data. J. Sediment. Res. 83, 954–961.
Yalin, M.S., 1963. An expression for bed-load transportation. J. Hydraul. Div. 89, 221–250.